



Models of high velocity impacts into dust-covered ice: Application to Martian northern lowlands

A. Reufer^{a,*}, N. Thomas^a, W. Benz^a, S. Byrne^b, V. Bray^b, C. Dundas^b, M. Searls^c

^a University of Bern, Physics Institute, Sidlerstrasse 5, 3012 Bern, Switzerland

^b University of Arizona, Lunar and Planetary Lab, Tucson, AZ 85721, USA

^c LASP, University of Colorado, Boulder, CO 80303-7814, USA

ARTICLE INFO

Article history:

Received 17 November 2009

Accepted 12 April 2010

Available online 24 April 2010

Keywords:

Mars craters

Hyper-velocity impacts

Liquid water Mars

Smoothed particle hydrodynamics

ANEOS

ABSTRACT

The detection of fresh impact craters with bright floors and ejecta (arising from fresh clean water ice) in the northern lowlands of Mars (Byrne et al., 2009b, *Science* 325, 1674), together with observations of polygonal structures and evidence from the Phoenix probe, suggests that there are substantial water ice deposits just below the surface over large areas. Specifically in cases of the larger craters observed, the impacts themselves may have raised the temperature and the pressure of the water ice deposits locally to values which allow phase changes. In this paper, we use smoothed particle hydrodynamics to model hyper-velocity impacts. We estimate peak shock pressures in a solid water ice target covered by a layer of loose material, modeled by pre-damaged dunite. In addition, we account for the possibility of a thin layer of sub-surface water ice by using a three-layer model where the ice is surrounded by dunite. We find that the peak shock pressures reached in the simulated events are high enough to produce several 100–1000 kg of liquid water depending upon the impact parameters and the exact shock pressure needed for the phase change. A difficulty remains however in determining whether liquid is generated or whether a type of fluidized ice is produced (or indeed some combination of the two). We also note that the process can become rather complex as the number of layers increases because of reflections of the shock at sub-surface boundaries—a process which should lead to increased fluidization.

© 2010 Elsevier Ltd. All rights reserved.

1. Introduction

Observations from the neutron and gamma-ray spectrometers, onboard the Mars Odyssey spacecraft, have shown that the upper most decimetres of the Martian northern lowlands contain large amounts, possibly exceeding 50% by mass, of a hydrogen-bearing molecule (widely inferred to be H₂O) poleward of $\pm 60^\circ$ latitude (Boynton et al., 2002; Feldman et al., 2002, 2004; Mitrofanov et al., 2002). The H₂O is assumed to be covered by a thin desiccated layer of fines and lightly consolidated material which prevents direct, unambiguous spectroscopic identification. The ubiquitous presence of periglacial landforms in the northern lowlands has been documented by many authors (Milliken et al., 2003; Mellon et al., 2008; Levy et al., 2009) and suggests that H₂O is in the form of ice in these regions. The existence of polygonal structures and “scallop” (Lefort et al., 2009) strongly supports the idea that desiccation produced by sublimation of ice in the upper most layer of the Martian soil is a global phenomenon.

Further support for this hypothesis has been provided by observations from the Phoenix probe which landed at 68°N. The

robotic arm and scoop were used to dig through this top layer. The Robotic Arm Camera (Keller et al., 2008) showed a mix of ice-cemented soil and relatively clean ice which was confirmed as being water ice by the evolved gas analyzer (Smith et al., 2008; Sutter et al., 2009). Evidence that the Phoenix site is not a singularity in the northern lowlands is currently being provided by the High Resolution Imaging Sciences Experiment (HiRISE; McEwen et al., 2007) onboard NASA's Mars Reconnaissance Orbiter (MRO).

Byrne et al. (2009a,b) have used HiRISE to study fresh impact craters, identified using the Context Imager (CTX) on MRO (Malin et al., 2007), at high resolution (25 cm/px). Five impacts in the northern mid-latitude lowlands were shown to have excavated several decimeters of material and exposed bright, relatively blue deposits strongly indicative of water ice. Although the craters produced were below the resolution limit of the Compact Reconnaissance Imaging Spectrometer for Mars (CRISM; Murchie et al., 2007), at one site sufficient material had been exhumed to provide an unambiguous signal of water ice.

Surficial water ice is not stable at these latitudes. Monitoring by HiRISE suggests that the surface area covered by clean water ice is shrinking with time, demonstrating that surficial water ice is not stable at these latitudes. The most natural hypothesis is that ice is being lost through sublimation (although it is difficult to

* Corresponding author. Tel.: +41 31 631 44 24; fax: +41 31 631 44 05.
E-mail address: andreas.reufer@space.unibe.ch (A. Reufer).

rule out coverage by fines as a means of obscuring the ice) and has been modeled by Dundas and Byrne (2010). Hence, these features are transient on timescales of a few months.

Several of the craters observed by HiRISE appear to have flat floors. This is contrary to what one would expect from impact into a structurally and chemically homogenous medium where bowl-shaped essentially hemispherical structures should result for the crater diameters in question.

Impact induced phase changes in the water ice change the behavior of the material during the cratering process, it is therefore natural to try to estimate the amount of water ice which undergoes phase changes in such impact events. One idea would be the production of liquid water in large amounts which later refreezes and directly produces a flat and clean water ice crater floor. The formation of such a pool of liquid water is not assured because the liquid can drain relatively quickly through a heavily fractured crater floor. However, a relatively thick solid ice layer which is not penetrated by the impact may prevent this. Another more important effect of liquid water during the cratering process is the change of the water ice material parameters. The coefficient of friction for damaged water ice changes dramatically if it is partially melted (Senft and Stewart, 2008). Such a mixture of solid and liquid water flows much more easily compared to purely solid ice and will exhibit different behavior at the later stages of crater formation.

It is reasonable to assume that we have a desiccated loose layer above an ice layer below. The ice layer may be relatively thin such that the impact can penetrate it completely and continue into a harder substrate below. Evidence that the ice layer is thin has been presented by Byrne et al. (2009a,b) and it may be a natural consequence of the sublimation and desiccation process. If the surface layer is relatively porous, the sublimed water vapor need not only to escape to the atmosphere but will also migrate to lower, cooler levels to build-up a denser layer of ice. Such behavior has been modeled extensively in studies of cometary nuclei (DeSanctis et al., 2007) and observed in the KOSI experiments (Benkhoff et al., 1995). An alternative explanation is that the thin layer results from the deposition process.

In order to investigate the crater formation process, to study the effects of different materials and their distribution with depth on crater formation and to place constraints on the formation of liquid water at the time of the impact, we have sought to model the impacts by using an established hydrocode.

Two different types of model are presented: A two-layer simulating an infinitely thick water ice layer covered by a layer of Martian regolith will be discussed first. We then investigate a three-layer model in which the water ice layer is relatively thin and surrounded by silicate-like material. In Section 2, we will describe our method, the numerical approach, the boundary conditions and the free parameters we use. In Section 3, we describe the most significant results of the simulations and compare shock attenuation to other theoretical and experimental work. Finally, in Section 4, we try to assess the amount of liquid water production and discuss these results in the context of the observations. We also discuss the effect of multiple layers on the ejection of material out of the crater.

2. Approach and boundary conditions

2.1. Approach

In hyper-velocity impacts into solids, a strong shock wave is created on contact between the impactor and the target (Melosh, 1989). Part of the kinetic energy is irreversibly transferred to heat and may melt or even vaporize water ice present below the

Martian surface. If adiabatic release from the shocked state is assumed and the Hugoniot known, the post-shock thermodynamic state of the ice and therefore the amount of melt, liquid and vapor can be determined with the entropy method (Ahrens and O'Keefe, 1972; Stewart and Ahrens, 2003).

2.2. Method

To model the early stage of the impact, we employ the Lagrangian method *smoothed particle hydrodynamics* (SPH, Monaghan, 1992) as a numerical technique. Particles represent smoothed out parcels of a continuum. Physical quantities like density and pressure are smoothed out by a kernel function around each particle with a length scale called the smoothing length h , so the spatial resolution of the method is proportional to this smoothing length. The resolution varies depending upon the problem: While weak gradients of the physical quantities like density or pressure can normally be resolved down to a length scale of $2h$, for more complicated problems like strong shocks this can only be done down to a scale of $7h$.

In most cases SPH is used to model fluids. Here we deal with a solid, which we model as an elastic continuum by solving the standard hydrodynamical equations under a full stress tensor. We further use Hooke's law model in which the deviatoric stress tensor is proportional to the strain rate.

Brittle failure of the solid is treated by introducing damage D ($0 \leq D \leq 1$) as a state variable for each SPH particle, reducing its strength under tensile loading. A particle with $D=0$ possesses full strength, reduced strength for $0 < D \leq 1$ and no strength at all for $D=1$. The latter case corresponds to the description of a fluid. The damage variable is evolved according to a fracture model based on work by Grady and Kipp (1980) and modified by Benz and Asphaug (1994). The underlying assumption is, that the solid has incipient flaws and that the number density of flaws per unit volume with a failure strain lower than a certain strain ε follows a power law, the Weibull (1939) distribution. This distribution has two free parameters which depend on the material modeled.

Individual flaws are initially distributed randomly amongst the SPH particles and each have an associated activation strength according to the Weibull distribution. If the current strain of a particle exceeds its flaw's activation strain because of stress, the flaw is activated and the growth of a crack is simulated by increasing the damage variable on a timescale given by the typical volume of the flaw and the crack growth velocity in the order of the speed of sound.

As an implementation of the model, we use the parallelized *ParaSPH* code.

2.3. Simulation setup

To model the Martian surface layer, SPH particles are initially placed on a hexagonal close-pack lattice filling a half-sphere at rest centered on the point of impact. The top layer of the half-sphere consists of a regolith-like layer with its thickness as a free parameter.

The number of materials for which we have a reliable equation of state and other parameters such as bulk modulus, shear modulus and the Weibull parameters, is relatively small. Of these, we choose dunite with an initial damage of 90% as a proxy material for the presumably loose Martian soil (Arvidson and Mellon, 2008; Moore et al., 1999).

In the two-layer model dunite is used for the surface layer and everything below is modeled as undamaged, pure, non-porous, water ice (compare Fig. 1a). Surface layer thickness has been

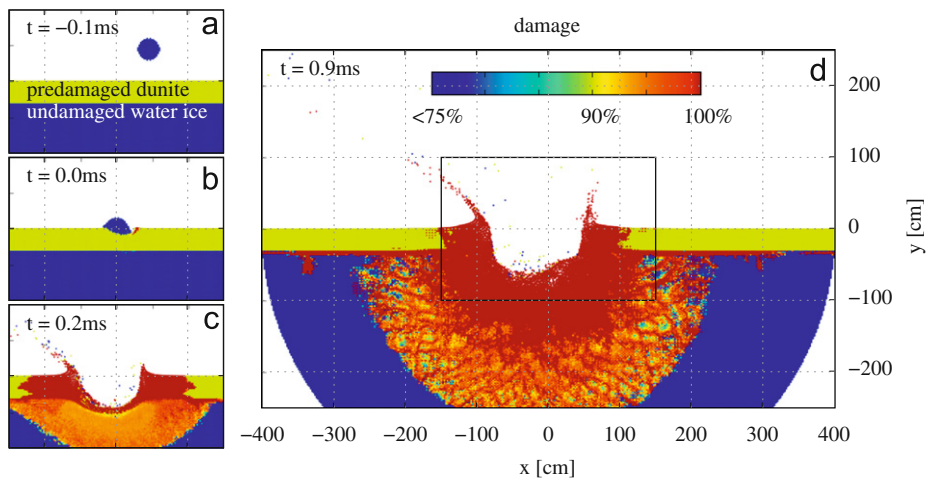


Fig. 1. Series of cuts along $y=0$ through snapshots at four different times for a 50 kg, 7 km/s impact onto a 90% predamaged and 30 cm thick surface. The damage state variable is color coded. Panel a shows the initial condition for the simulation, panel b the actual impact. In panels c and d, the shock wave passes through the water ice and the following rarefaction wave leaves the ice damaged. In the beginning the rarefaction wave is still strong enough to completely damage the water ice as it can be seen just around the forming impact crater where damage amounts 100%. Further out, only the weakest flaws are activated, leaving a complex fractured structure.

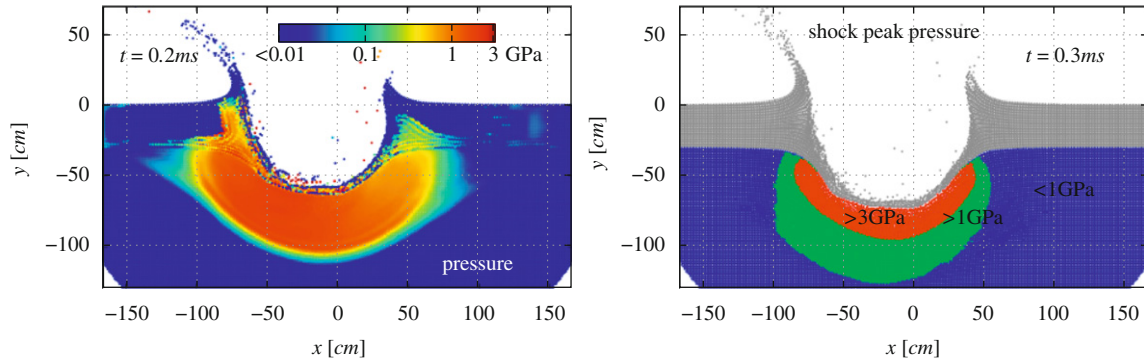


Fig. 2. Two cuts along $y=0$ for snapshots at two different times for a 50 kg, 10 km/s impact onto a two-layer model with a 90% predamaged and 30 cm thick surface. The left plot shows color coded the actual pressure at $t=0.3$ ms: an almost spherically symmetric shock wave propagates from the now displaced center of impact into the ice layer. Due to a higher speed of sound in the dunite layer, a weak conical precursor wave is refracted into the ice phase. Note the lack of pressure where the material is fully damaged, notably in the surface layer. The right plot shows the peak shock pressures at a time, where the shock wave already has decayed below 1 GPa. Red color represents ice shocked to a least 3 GPa, green ice shocked at least to 1 GPa, blue ice shocked below 1 GPa and grey represents dunite.

chosen to be $d=0, 10, 20, 30$ and 60 cm. Fig. 1a shows the initial setup for a two-layer model with a 30 cm thick surface (Fig. 2).

In view of the postulated ice layer at a shallow depth (Byrne et al., 2009a, b), we also investigate a three-layer model. Here, the middle layer is composed of pure water ice with a thickness $d_{ice}=60$ cm and a lower layer of pre-damaged dunite again (compare Fig. 3).

For both materials in the model (dunite and water ice) we use the ANEOS (Thompson, 1990) equation of state which covers basic phase transitions. Note that while all layers possess their materials corresponding strength, no strength is modeled between the individual layers.

The impactor is modeled by a homogenous sphere of undamaged dunite. Both the target and the impactor are initially in equilibrium. Gravity and the thin atmosphere on Mars are neglected. While the atmosphere is important for the stability of liquid water, its pressure of a few hPa (Schofield et al., 1997) is negligible compared to the shock pressures of several GPa in the relevant region and can therefore be neglected during the simulated early stages of the impact.

As will be shown in the discussion, literature values for the peak shock pressure needed for incipient melting under Mars surface conditions vary considerably. The lowest estimates for

pure water ice lie around 1 GPa. Even for the most energetic impact parameters considered here, the peak pressure dropped below 1 GPa at distances in the order of 2 m from the point of impact or around 1 ms after the impact. So in order to capture all produced melt and liquid, the shock wave has to be followed for 2 m and at least 1 ms after impact, which sets a minimal size for the computational volume to be used in the simulation. We use three different resolutions, by keeping the SPH particle number constant, but by varying the radius of the half-sphere used to model the Martian surface. Simulations with a low resolution use a half-sphere radius of $r=8$ m ($h=7.0$ cm), medium resolution $r=4$ m ($h=3.5$ cm) and high resolution $r=2$ m ($h=1.7$ cm).

Both, the target and the impactor, have an initial temperature of 240 K, which corresponds to the assumed mean temperature at the impact sites (Schofield et al., 1997). More recent models indicate a lower 200–210 K (Dundas and Byrne, 2010). The end result does not strongly depend on the exact value of the initial temperature, as the difference in internal energy (2.05 J/gK, Lide, 1994) between the two cases only represents 20% of the latent heat for water ice (333 J/g).

For all simulations we use the same 45° impact angle. For impacts which are not too oblique, the cratering process does not depend significantly on the impact angle (Melosh, 1989).

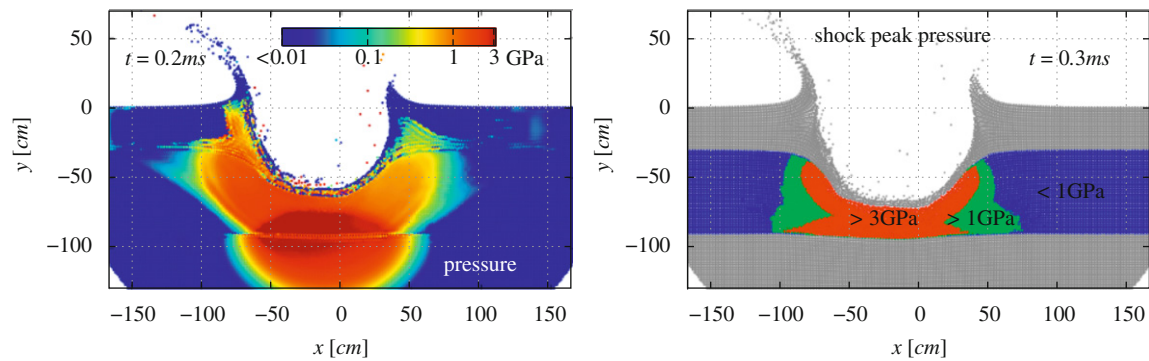


Fig. 3. Same two cuts as above in Fig. 2 for the same impactor parameters, but into a three layer model. Compared to the two layer mode, the ice layer here is of finite thickness. Below the buried ice layer there is pre-damaged dunite again. When the shock wave hits dunite again after having passed through the ice, it is partially reflected back into the ice with a even higher pressure due to the higher bulk modulus of dunite. As a consequence, more water ice is shocked to the pressures needed for melting. Furthermore, in some region the water ice is shocked several times by strong shock waves as they bounce back and forth between the transitions between ice and dunite.

Impactor parameters have been varied between a mass of 25, 50 and 75 kg and a velocity of 7, 10 and 15 km/s. Neglecting atmospheric braking, the Mars escape velocity sets a lower limit of 5 km/s for the impact velocity. The expected average impact velocity of asteroids is 9.6 km/s (Ivanov, 2001).

2.4. Limitations

The method applied here can only be used for the contact and compression phases of the impact. Once the shock wave reaches the boundary of the computational volume, it is reflected back into it which is a numerical artifact and a deviation from the physical situation to be modeled. To make sure the results are not affected by this artifact, the simulations have to be stopped before the reflected waves reach the region of interest. This does not affect the results for the peak shock pressure, as the reflections always occur after the shock wave has decayed below interesting pressures. Another limitation is that the later cratering processes cannot be simulated, due to the inability to model the behavior of the granular impact debris. A final crater profile therefore cannot be determined. Nevertheless with our method the peak shock pressures reached in the water ice can be determined.

3. Results

3.1. Principal characteristics

Fig. 1a–d show a series of snapshots at different times for a typical simulation. The impactor sphere can be seen in panel a slightly before and in panel b at the time of impact. At contact with the surface, the impactor starts to compress the underlying material and a crater starts to form. As the speed of sound in dunite is larger than in water ice, a shock wave travels horizontally along the surface layer. The following rarefaction wave leaves a ring of completely damaged dunite around the forming crater. In the water ice, the shock wave propagates spherically around the point of impact. The rarefaction wave leaves a much larger volume damaged because of the lower strength of the water ice compared to dunite.

3.2. Shock attenuation

The pressure of a spherical shock wave in a homogenous solid, if above the Hugoniot elastic limit, decays according to a power law $P_{peak}(r) = P_0(r/r_0)^{-a}$ due to attenuation (Pierazzo et al., 1997; Shirai et al., 2008; Melosh, 1989). In the strong shock regime,

where the stresses strongly exceed the term $\rho_0 C_0^2$ (ρ_0 : density, C_0 : speed of sound, both at zero stress), attenuation parametrized by a reaches the highest value. For water ice this is the case above $\rho_0 C_0^2 \approx 0.9$ GPa (Mitani, 2003). Shock waves with stresses around that value are considered to be in the intermediate or material strength regime with a lower attenuation. Below the intermediate lies the weak shock regime, even weaker waves then become acoustic. The decrease in attenuation rate can be seen in our peak shock pressure profiles in Fig. 6: Except for the lowest resolution simulations, a slight kink in the slopes of the red (high resolution) and green curves (medium resolution) can be observed. For the intermediate shock regime, we obtained values $a_1 = 1.73 \dots 2.31$ comparable to literature values for non-porous materials (Mitani, 2003). Pierazzo et al. (1997) find a value of 2.1 for a direct 10 km/s impact into water ice, with a power-law dependence on impact velocity.

For higher resolutions, we get higher attenuation rates, which can be explained by better resolved shock wave and the higher peak shock pressures reached.

Table 1 shows the amount of water ice shocked to a higher pressure than 1 and 3 GPa for a set of low-resolution simulations. Examples of mass histograms for high velocity impacts with 15 km/s are shown in Fig. 4. As with the peak shock pressure profiles, the mass histograms show a power law dependence on pressure with different slopes. Under the assumption of a spherical symmetric shock wave and a constant exponent a , the mass M shocked to a certain pressure P is simply given by resolving the peak shock pressure power law from above for r and putting it into the mass of a half-sphere: $M(P) = V(P)\rho = (3/2)\pi\rho r_0^3(P/P_0)^{-3/a} \sim P^{-3/a}$.

Especially for the high pressure end of the mass function the assumptions break down. The highest pressures in the ice are reached at the interface, where the original shock wave in the dunite gets coupled into the water ice in a non-trivial way. Due to an impedance mismatch, the shock wave is refracted and becomes non-spherical. Another reason is the non-constant attenuation exponent a , which lets the mass function deviate from a simple power law.

3.3. Dependence on parameters

The peak shock pressures show almost no dependence on the initial damage assigned to the surface dunite layer. Varying the damage between $D = 0 \dots 1$ only changes the mass function by a few percent. This is because the tensile strength, which is directly reduced by damage, mostly affects the rarefaction wave and the cratering processes at later stages, but not the shock wave itself.

Table 1

Mass of ice shocked to at least 1 and 3 GPa for some low resolution ($h=7$ cm), two-layer simulations with different impact parameters and surface thicknesses. Note that numerical convergence has not been reached with these simulations. The values can be used to compare different parameters under the same resolution and serve as a lower limit, as the peak shock pressures converge to higher values for better resolved simulations.

Impactor		Surface thickness (m)	Ice mass shocked to	
Mass (kg)	Velocity (km/s)		$P \geq 1$ GPa (kg)	$P \geq 3$ GPa (kg)
25	10	0.0	912.4	220.9
		0.1	580.3	112.8
		0.6	0.0	0.0
50	10	0.0	2260.1	627.5
		0.1	1677.7	423.9
		0.2	1001.6	210.0
		0.3	561.2	87.6
		0.6	127.0	0.0
75	10	0.0	3550.4	1062.9
		0.1	2750.6	738.9
		0.2	1761.7	412.3
		0.3	1076.4	220.4
		0.6	391.3	18.9
25	15	0.1	1627.1	405.7
		0.2	1075.2	244.5
		0.3	625.6	110.9

Therefore only results with an initial damage $D=0.9$ are shown here.

The surface layer permits the shock wave to be attenuated and its thickness directly sets the peak pressures of the shock wave once it reaches the water ice. This can be seen for example in Fig. 4 where for given impactor parameters the mass functions for different surface thicknesses are shown: The mass functions are just shifted in mass, but show the same characteristics independent of the surface thickness. The kinetic energy K determined by the velocity and mass of the impactor sets the energy available to the impact event and the shocking of the water ice. The partitioning of velocity and mass is only of minor importance, as can be seen for example when comparing the 50 kg with 10 km/s impactor case ($K=2.5$ GJ, Fig. 5) and the 25 kg with 15 km/s case ($K=2.8$ GJ, Fig. 4), both having a surface depth of 30 cm and a resolution of $h=7$ cm: The mass functions are almost identical except for the high pressure tail where other factors such as the different sizes of the impactors play a role. For thinner surfaces, the 15 km/s case shows slightly higher masses due to higher initial shock pressures reached. For thicker surfaces the effect diminishes.

3.4. Resolution issues

Fig. 5 shows the mass functions for different resolutions for two choices of the other parameters. The resolution is proportional to the smoothing length h . Strong shock waves can be resolved roughly down to a length scale of $\approx 7h$. The resolution has been doubled twice from a smoothing length of $h=7$, to 3.5 cm and again to 1.8 cm. It can be clearly seen that numerical convergence is not fully accomplished, although a clear trend is visible. This is because the pressure in a strong shock wave is a very steep function. While the overall characteristics of the shock wave are correctly reproduced under low-resolution, the pressure peak is smoothed out and the peak pressure reached is

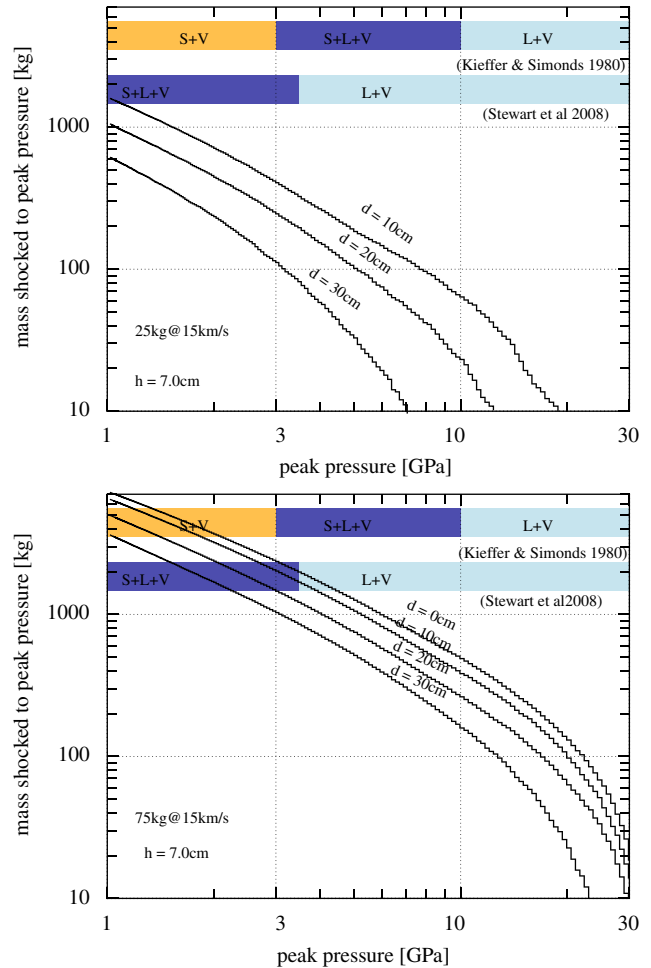


Fig. 4. Ice mass shocked to a certain pressure as a function of pressure for the low-resolution, two-layer simulations ($h=7$ cm) with a 15 km/s impact velocity and an impactor mass of 25 kg (top) and 75 kg (bottom).

underestimated. Hence, the values obtained for the shocked ice masses can be regarded as lower bounds. Unfortunately the values for the peak pressure do not converge along a simple function depending on resolution (Jutzi, 2009). It is therefore not possible to extrapolate the converged value for the peak pressure by fitting a scaling law to the obtained values for different resolutions. Note that the shock profiles (Fig. 6) show much less difference in pressure. The much larger differences in the mass functions arise due to the strong r^3 -dependence on radius and the relatively flat shock profiles.

3.5. Three-layer models

For a 50 kg impactor with a velocity of 10 km/s, a three-layer model was also run. As can be seen in Fig. 3, a 60 cm thick pure ice layer is buried under the 30 cm thick, pre-damaged dunite surface layer. The only difference to the corresponding two-layer model is the additional dunite below the ice layer. This additional change in material has the effect of a partial reflection of the shock wave back into the ice again, as can be seen in Fig. 3. The reflected shock wave actually has a higher pressure than its predecessor. As a result, more ice is shocked to high pressure, so more melt and liquid can be expected. In this model, the ice layer is passed by shock waves several times, making the determination of the thermodynamic evolution after shock release more difficult. It is no longer possible to determine the end state by a simple peak

pressure reached in the ice. Nevertheless it can be said that much more water ice is partially or completely melted compared to an impact with the same parameters into the corresponding two-layer model, as every passing of a shock wave just increases the entropy in the shocked material. Table 3 gives the masses reaching at least 1 and 3 GPa. Note that the required peak shock pressure needed for melting is actually lower, when the ice gets

shocked several times to that pressure, compared to the case when the ice is only shocked once.

4. Discussion

4.1. Liquid phase production

Out of the simulations, we only get the peak pressures reached in the water ice. From that we can estimate the amount of produced liquid water. The pressure needed to liquify water ice under Martian surface conditions depends on many parameters. For pure, non-porous ice, the material considered in the simulations here, the literature values vary considerably.

Early work by Kieffer and Simonds (1980), using the entropy method, determined the required shock pressure to be > 3 GPa for incipient and > 10 GPa for complete melting. Part of the water ice will end up in the vapor phase, with complete vaporization > 100 GPa.

More recent experimental work by Stewart and Ahrens (2003) found incipient melting upon shock release > 4.5 GPa and complete melting > 5.5 GPa for solid water ice at 100 K. For 40% porous ice at 150 K shock pressures as small as > 0.3–0.5 GPa are enough for incipient and > 2 GPa for complete melting. For higher initial temperatures between 150 and 275 K incipient melting starts at pressures as low as 0.6–2.2 GPa (Stewart-Mukhopadhyay, 2002), with lower pressure for higher initial temperature. Senft and Stewart (2008) worked on Martian impacts in water ice at 210 K and 6 mbar which are similar to our initial conditions (240 K, 6 mbar). They found pressures for incipient melting > 1 GPa and complete melting > 3 GPa. We use these pressures as they match our initial conditions best. We give shocked ice masses at these values in Tables 1–3. Due to our 30 K higher initial temperature for the water ice, the shocked ice masses may actually be slightly underestimated by using the values by Senft and Stewart (2008).

Although not considered in these simulations, for mixtures of water ice and rocky materials as in permafrost, the needed pressures for melting may be higher compared to pure water ice (Ivanov et al., 2005). This is important, as such a mixture may present a more realistic situation than the pure layer modeled in our simulations although we note the purity of the ice derived by Dundas et al. (2009). It also means that melting and refreezing permafrost as a way of producing clean ice requires higher peak shock pressures than for melting pure ice.

Similarly Kraus et al. (2009) investigated 60:40 volumetric mixtures of water ice and quartz sand at a temperature of 263 K and a pressure of ≈ 1 Pa. With shock pressures from 7.9 to

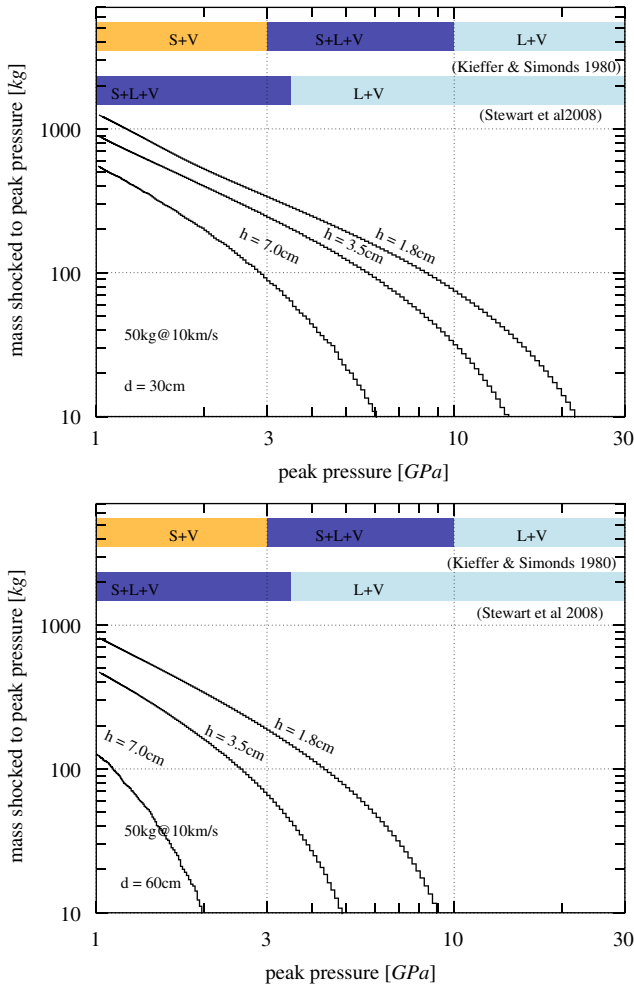


Fig. 5. Shocked ice mass functions for 50 kg impactor with 10 km/s for two different surface thicknesses and different resolutions. Numerical convergence has not been reached, but a trend towards higher peak shock pressures for higher resolutions is apparent.

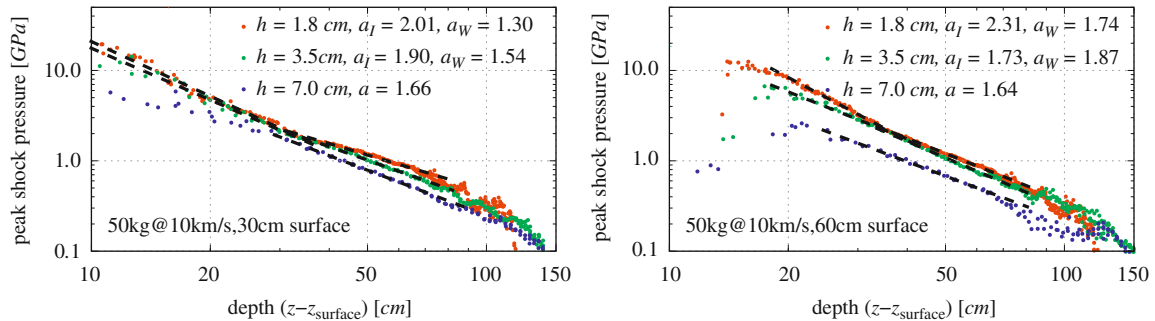


Fig. 6. Resolution dependent peak shock pressures along a slab $[-25 \text{ cm} \pm 2h, 0 \text{ cm} \pm 2h, z]$ for a 50 kg impact with an impact velocity of 10 km/s on a 30 cm surface (left plot) and a 60 cm surface (right plot) at 0.5 ms after the impact, only ice particles are plotted (compare the right plot of Fig. 2 for a full snapshot for the 30 cm case). The depth is measured relative to the surface at the moment of the snapshot (z_{surface}). The slab is chosen such that the distance between the ice layer and the point of impact is the smallest and therefore the shock wave has experienced the least amount of damping. Fitting power law ($P_{\text{peak}}(z) = P_0(z/z_0)^{-a}$) exponents a are shown for the different resolutions. All resolutions except for the lowest one show a slight kink and a change of slope between the intermediate and the weak shock regime around 2 GPa.

Table 2

Resolution dependent mass of ice shocked to a certain pressure for a 50 kg impactor with 10 km/s on a two-layer model. The smoothing length h is proportional to the resolution. A clear trend works towards higher masses for higher resolutions.

Surface thickness (m)	Smoothing length h (cm)	Ice mass shocked to	
		$P \geq 1$ GPa (kg)	$P \geq 3$ GPa (kg)
0.3	1.8	1279.0	335.3
	3.5	906.9	242.6
	7.0	561.2	87.6
0.6	1.8	834.6	185.8
	3.5	482.0	65.3
	7.0	127.0	0.0

Table 3

Resolution dependent amount of ice shocked to a certain pressure for a 50 kg impactor with 10 km/s on a three-layer model. More ice is shocked to the given pressures compared to the two-layer simulations with the same impactor parameters (2).

Surface thickness (m)	Smoothing length h (cm)	Ice mass shocked to	
		$P \geq 1$ GPa (kg)	$P \geq 3$ GPa (kg)
0.3	1.8	1357.4	448.2
	3.5	997.2	283.2

22.7 GPa they reached temperatures after adiabatic release of 630–1220 K.

Overall we can say that even when assuming conservatively high shock pressures needed for melting water ice, the impact events considered here easily lead to incipient melting of several hundred and complete melting of up to a few hundred kilograms of water ice (compare Tables 1 and 2).

4.2. Damaged ice

Strong elastic waves or shock waves with a mean pressure above the Hugoniot-Elastic Limit (HEL) lead to a complete failure of solid material. For water ice, Kato et al. (2001) give a value for the HEL between 0.1 and 0.3 GPa. Stewart et al. (2008) estimate a higher 0.5 GPa.

The HEL lies well below the pressures needed for melting or vaporizing the water ice, therefore much more damaged than melted water ice is produced. Fully damaged water ice behaves like a granular media and has a low coefficient of friction, especially when partially melted or near the melting point (Senft and Stewart, 2008). Flows of such a mixture late in the cratering process might also settle under gravity and later refreeze to a flat ice surface, producing the observed flat crater floors.

4.3. Ejecta

For impacts into a homogenous target, different ejection mechanisms are expected (Melosh, 1989): Jetting ejects impactor and target surface material sideways at a high velocity during the contact phase. When the shock wave caused by the impactor propagates inside the target and hits the free surface, spallation of surface material occurs. At the later excavation stage, material from the surface or small depths is ejected at small velocities. All those types cannot eject material which originally was buried

under the point of impact or in other words, where our simulations show production of water ice melt and liquid water.

In the three layer model presented here, another ejection process is possible: As the shock wave propagates downward through the ice and reaches the boundary to the underlying dunite layer, the impedance mismatch between the two solids causes a compressional wave to be reflected back into the ice (compare left panel of Fig. 3). This wave has a particle velocity pointing upwards, making it possible to eject water ice directly from the crater. While our simulations show upward velocities for the ice in the three-layer models as expected, it is difficult to estimate the final ejection velocities as the simulations model a much shorter timescale, than the ejected water ice needs to escape the crater.

4.4. Comparison with observations

Byrne et al. (2009a,b) present five cratering sites with impacts between July 2004 and September 2008. With Pi-group scaling (Melosh, 1989; Holsapple, 1993; Richardson et al., 2007) we can estimate the impact energies required to produce the observed craters. From that, assuming an impact velocity, we can also determine the required impactor masses and compare the craters with our impact simulations. The ice layer depths are obtained from a model by Mellon et al. (2004) with updated values in Byrne et al. (2009a,b).

Table 4 compiles expected impactor masses for different target materials taken from Richardson et al. (2007). We assumed a rocky impactor with a density of 3 g/cm³, Martian gravity, no atmosphere and an impact velocity of 10 km/s and an angle of 45°. While the layered Martian surface cannot be approximated by any of the chosen materials, they give a rough idea of the impact conditions and allow us to compare the craters with the simulations.

The loose uppermost layer of the Martian surface is best matched by sand as a target material. Below the relatively pure ice layer, the soil is expected to form an impervious mixture of soil and amounts of ice. The strength of this ice-cemented soil is higher than for pure ice (Hiraoka et al., 2008) and its density is lower than for most soils. We assumed an effective strength of 1 MPa. Density is higher compared to most soils, due to the low porosity. The derived impactor masses should lie somewhere between the values derived for pure ice and for alluvium.

Impact site 1 shows crater depths just as deep as the modeled ice layer depth, so cratering happens almost exclusively in the loose surface material. For a sand target, an impactor of 2 kg with 10 km/s is required to produce the observed crater. Comparing that with the simulations shows no melt or liquid production, especially as at this site the ice layer is expected to be buried quite deep.

Table 4

Recently observed impact craters (Byrne et al., 2009a,b) and their modeled ice depths (Mellon et al., 2004; Byrne et al., 2009a,b). Impactor masses are obtained through Pi-scaling (Holsapple, 1993; Holsapple and Housen, 2007; Richardson et al., 2007) by assuming loose sand, alluvium and solid ice for the target material. An initial crater depth to diameter ratio of 0.25 was assumed. Note that the crater depth for site 3 was not actually measured but inferred to be $0.2 \times$ the crater diameter.

Impact site	1	2	3	4	5
Crater diameter (m)	4	6	8	6	12
Crater depth (m)	0.55	1.33	1.6	1.76	2.46
Modeled ice depth (m)	0.51	0.74	0.12	0.38	0.14
Imp. mass (kg) (for 10 km/s)					
Sand	2	8	23	8	100
Ice	4	13	32	13	108
Alluv.	7	23	56	23	200

Sites 2–5 have crater depths penetrating past the expected ice depth, especially sites 3 and 5 where the ice layer is near the surface. Here, most of the cratering takes place below the ice layer and the impactor masses are anticipated somewhere between the ones for ice and alluvium.

Comparing sites 2 and 4 with the low-resolution two-layer simulation with the 25 kg impactor into the buried ice layer at 0.6 m depth (compare Table 1), suggests that no phase changes in the ice would be expected. The impactor masses are too small and the ice is buried too deep.

Sites 3 and 5 are more promising. Phase changes are expected for a considerable amount of ice, as the ice layer is assumed to be nearer to the surface compared to the other sites. Although site 3 has a rather small crater caused by an impactor with the mass of a few tens of kg, the two-layer simulations with 25 and 50 kg impactors into an ice layer buried 0.1 m deep, show that more than 1000 kg of melt and several 100 kg of liquid water can be expected. Note that the values derived from the two-layer simulations are probably an exaggeration, as they assume an ice layer with an unlimited thickness. If the ice layer is only thin, the amount of melt and liquid will be limited by the amount of solid ice available in the ice layer.

In the case of site 5 (compare HiRise picture PSP_010861_2265 in Fig. 7), the largest of the five craters, large parts of the buried ice layer can be melted and liquified by the impact. This is immediately evident from the simulations with high impactor masses.

4.5. Stability of liquid water on Mars

Liquid water is not stable under Martian conditions, as the atmospheric pressure lies below the triple point of water. But it can be metastable for several hours under Martian surface

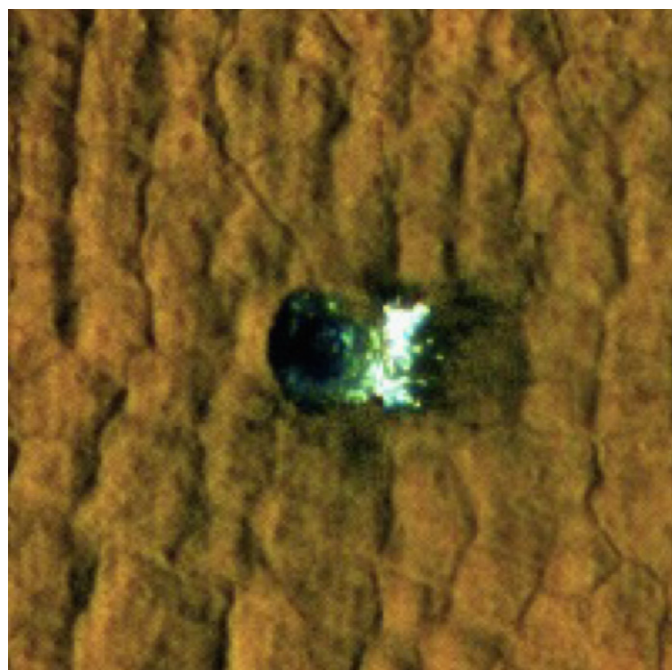


Fig. 7. Part of HiRise picture PSP_010861_2265 (Credit: NASA/JPL/University of Arizona) showing a fresh impact formed between July 2004 and June 2008 at a latitude of N46.16° near Arcadia Planitia. The crater diameter is 12 m and the depth measured from shadows is expected to be 2.4 m (Byrne et al., 2009a,b). The white spots show spectral signatures of water ice. Inside the crater, decimeter sized spots of ice can be seen. Compared to other recently observed impacts site, the relative absence of icy spots at the crater floor suggests that the crater has excavated completely through an ice layer close to the surface.

conditions as shown by Hecht (2002). This timescale is much larger than required for fluid flow. Hecht determined that an open pool of liquid water will show evaporation rates of only a few mm/h. In the case of relatively pure water, a thin ice crust will form on the surface and inhibit evaporative cooling in the underlying liquid phase. Impurities in the water also lower the melting point and increase the freezing time scale. Considering the evaporation and freezing timescales, liquid water produced in such impact events as shown here has enough time to drain into cracks or available pore space.

Salinity which according to Tosca et al. (2008) reaches high values on Mars, also considerably lowers the melting point of liquid water and may increase the time until the liquid water freezes again.

Conduction could significantly accelerate freezing, but the soil within the crater will also be warmed by the impact.

4.6. Uncertainties

As mentioned above, numerical convergence for the mass functions has not been reached. As the shock wave is not being resolved well enough, the peak of the pressure gets smoothed out and the peak pressure value does not reach the real physical value. This means the estimated peak shock pressures are underestimated and the mass functions are shifted towards lower pressure as shown in Fig. 5. So the mass functions obtained here should rather be understood as lower bounds than exact results.

There are many unknowns in the comparison of the simulations with the observed craters. The Pi-scaling only gives rough estimates of the impact parameters, first of all due to the simplification of the model but also because of unknown target parameters. Nevertheless, significant amounts of liquid and melt can be expected for a wide range of different target parameters.

4.7. Summary and future work

The simulations presented here show that in the larger impact events on Mars as recently observed, significant amounts of a buried water ice layer can undergo phase changes. Although the fate of the liquid water produced is not clear, formation of decameter-scale craters provides an interesting source of liquid water.

Acknowledgements

We are grateful for interesting and valuable comments from the anonymous referee. This work was supported in part by the Swiss National Science Foundation. Computations were made on the ISIS2 cluster at the University of Bern.

References

- Ahrens, T.J., O'Keefe, J.D., 1972. Shock melting and vaporization of lunar rocks and minerals. *The Moon* 4, 214.
- Avidson, R.E., Mellon, M.T., 2008. Geologic setting and soil physical properties of the Mars phoenix landing site. AGU Fall Meeting Abstracts, A1+, December.
- Benkhoff, J., Seidensticker, K.J., Seiferlin, K., Spohn, T., 1995. Energy analysis of porous water ice under space-simulated conditions: results from the KOSI-8 experiment. *Planet. Space Sci.* 43, 353–361.
- Benz, W., Asphaug, E., 1994. Impact simulations with fracture. I—method and tests. *Icarus* 107, 98–116.
- Boynton, W.V., Feldman, W.C., Squyres, S.W., Prettyman, T.H., Brückner, J., Evans, L.G., Reedy, R.C., Starr, R., Arnold, J.R., Drake, D.M., Englert, P.A.J., Metzger, A.E., Mitrofanov, I., Trombka, J.L., d'Uston, C., Wänke, H., Gasnault, O., Hamara, D.K., Janes, D.M., Marcialis, R.L., Maurice, S., Mikheeva, I., Taylor, G.J., Tokar, R., Shinohara, C., 2002. Distribution of hydrogen in the near surface of Mars: evidence for subsurface ice deposits. *Science* 297, 81–85.

- Byrne, S., Dundas, C.M., Kennedy, M.R., Mellon, M., Shean, D., Daubar, I., Cull, S., Seelos, K.D., Murchie, S.L., Cantor, B., Arvidson, R.E., Edgett, K., McEwen, A.S., Harrison, T., Posiolova, L., Seelos, F.P., Hirise Team, Ctx Team, Crism Team, 2009a. Excavation of subsurface ice on Mars by new impact craters. In: Lunar and Planetary Institute Science Conference Abstracts. Lunar and Planetary Institute. Technical Report, vol. 40, pp. 1831–1832.
- Byrne, S., Dundas, C.M., Kennedy, M.R., Mellon, M.T., McEwen, A.S., Cull, S.C., Daubar, I.J., Shean, D.E., Seelos, K.D., Murchie, S.L., Cantor, B.A., Arvidson, R.E., Edgett, K.S., Reufer, A., Thomas, N., Harrison, T.N., Posiolova, L.V., Seelos, F.P., 2009b. Distribution of mid-latitude ground ice on Mars from new impact craters. *Science* 325, 1674.
- DeSanctis, M.C., Capria, M.T., Coradini, A., Ammannito, E., 2007. Thermal evolution models of the 9P/Tempel 1 comet nucleus for interpreting the deep impact results. *Astron. J.* 133, 1836–1846.
- Dundas, C.M., Byrne, S., 2010. Modeling sublimation of ice exposed by new impacts in the martian mid-latitudes. *Icarus* 206 (2), 716–728, doi:10.1016/j.icarus.2009.09.007.
- Dundas, C.M., Byrne, S., McEwen, A.S., 2009. Modeling sublimation of ice exposed by recent impacts in the Martian mid-latitudes. In: Lunar and Planetary Institute Science Conference Abstracts, Lunar and Planetary Institute. Technical Report, vol. 40, pp. 2168–2169.
- Feldman, W.C., et al., 2004. Gamma-ray, neutron, and alpha-particle spectrometers for the lunar prospector mission. *Journal of Geophysical Research* 109, E07S06, doi:10.1029/2003JE002207.
- Feldman, W.C., Boynton, W.V., Tokar, R.L., Prettyman, T.H., Gasnault, O., Squyres, S.W., Elphic, R.C., Lawrence, D.J., Lawson, S.L., Maurice, S., McKinney, G.W., Moore, K.R., Reedy, R.C., 2002. Global distribution of neutrons from Mars: results from Mars Odyssey. *Science* 297, 75–78.
- Grady, D., Kipp, M., 1980. Continuum modelling of explosive fracture in oil shale. *International Journal of Rock Mechanics and Mining Sciences Geomechanics Abstracts* 17 (3), 147–157.
- Hecht, M.H., 2002. Metastability of liquid water on Mars. *Icarus* 156, 373.
- Hiraoka, K., Arakawa, M., Setoh, M., Nakamura, A.M., 2008. Measurements of target compressive and tensile strength for application to impact cratering on ice-silicate mixtures. *Journal of Geophysical Research* 113, 02013.
- Holsapple, K.A., 1993. The scaling of impact processes in planetary sciences. In: *Annual Review of Earth and Planetary Sciences*, vol. 21 (A94-10876 01-91), p. 333.
- Holsapple, K.A., Housen, K.R., 2007. A crater and its ejecta: an interpretation of deep impact. *Icarus* 191, 586.
- Ivanov, B.A., 2001. Mars/moon cratering rate ratio estimates. In: 32nd Annual Lunar and Planetary Science Conference, vol. 32, p. 1249.
- Ivanov, B.A., Artemieva, N.A., Pierazzo, E., 2005. Impact cratering and material models: subsurface volatiles on Mars. In: *Workshop on the Role of Volatiles and Atmospheres on Martian Impact Craters*, vol. 1273, p. 55.
- Jutzi, M., 2009. Studies of collisions involving porous bodies. Ph.D. Thesis, Universitaet Bern.
- Kato, M., Higa, M., Shirai, K., Ichi Iijima, Y., Kiyono, T., Nakazawa, S., Arakawa, M., 2001. Shock pressure attenuation in water ice at a pressure below 1 GPa. *Journal of Geophysical Research* 106, 17567.
- Keller, H.U., et al., 2008. Phoenix robotic arm camera. *Journal of Geophysical Research* 113, E00A17, doi:10.1029/2007JE003044 [printed 114(E3), 2009].
- Kieffer, S.W., Simonds, C.H., 1980. The role of volatiles and lithology in the impact cratering process. *Reviews of Geophysics and Space Physics* 18, 143.
- Kraus, R.G., Stewart, S., Seifert, A., Obst, A.W., 2009. Shock and post-shock temperatures in an ice-quartz mixture: implications for melting during planetary impact events. *Geophysical Research Letters* 35.
- Lefort, A., Russell, P.S., Thomas, N., McEwen, A.S., Dundas, C.M., Kirk, R.L., 2009. Observations of periglacial landforms in Utopia Planitia with the High Resolution Imaging Science Experiment (HiRISE). *Journal of Geophysical Research* 114, E04005, doi:10.1029/2008JE003264.
- Levy, J., Head, J., Marchant, D., 2009. Thermal contraction crack polygons on Mars: classification, distribution, and climate implications from HiRISE observations. *Journal of Geophysical Research* 114, 01007.
- Lide, D.R., 1994. *CRC Handbook of Chemistry and Physics. A Ready-reference Book of Chemical and Physical Data*.
- Malin, M.C., et al., 2007. Context camera investigation on board the Mars Reconnaissance Orbiter. *Journal of Geophysical Research* 112, E05S04, doi:10.1029/2006JE002808.
- McEwen, A.S., et al., 2007. Mars Reconnaissance Orbiter's High Resolution Imaging Science Experiment (HiRISE). *Journal of Geophysical Research* 112, E05S02, doi:10.1029/2005JE002605.
- Mellon, M.T., Arvidson, R.E., Marlow, J.J., Phillips, R.J., Asphaug, E., 2008. Periglacial landforms at the phoenix landing site and the northern plains of Mars. *Journal of Geophysical Research* 113.
- Mellon, M.T., Feldman, W.C., Prettyman, T.H., 2004. The presence and stability of ground ice in the southern hemisphere of Mars. *Icarus* 169, 324.
- Melosh, H.J., 1989. *Impact Cratering: A Geologic Process*. adsabs.harvard.edu.
- Milliken, R.E., Mustard, J.F., Goldsby, D.L., 2003. Viscous flow features on the surface of Mars: observations from high-resolution Mars orbiter camera (MOC) images. *Journal of Geophysical Research (Planets)* 108, 5057.
- Mitani, N.K., 2003. Numerical simulations of shock attenuation in solids and reevaluation of scaling law. *Journal of Geophysical Research (Planets)* 108, 5003.
- Mitrofanov, I., Anfimov, D., Kozyrev, A., Litvak, M., Sanin, A., Tret'yakov, V., Krylov, A., Shvetsov, V., Boynton, W., Shinohara, C., Hamara, D., Saunders, R.S., 2002. Maps of subsurface hydrogen from the high energy neutron detector, Mars Odyssey. *Science* 297, 78–81.
- Monaghan, J.J., 1992. Smoothed particle hydrodynamics. *Annual Review of Astronomy and Astrophysics* 30, 543–574.
- Moore, H.J., Bickler, D.B., Crisp, J.A., Eisen, H.J., Gensler, J.A., Haldemann, A.F.C., Matijevic, J.R., Reid, L.K., Pavlics, F., 1999. Soil-like deposits observed by Sojourner, the Pathfinder rover. *Journal of Geophysical Research* 104, 8729–8746.
- Murchie, S., et al., 2007. Compact Reconnaissance Imaging Spectrometer for Mars (CRISM) on Mars Reconnaissance Orbiter (MRO). *Journal of Geophysical Research* 112, E05S03, doi:10.1029/2006JE002682.
- Pierazzo, E., Vickery, A.M., Melosh, H.J., 1997. A reevaluation of impact melt production. *Icarus* 127, 408.
- Richardson, J.E., Melosh, H.J., Lisse, C.M., Carcich, B., 2007. A ballistics analysis of the deep impact ejecta plume: determining comet tempel 1's gravity, mass, and density. *Icarus* 191, 176.
- Schofield, J.T., Barnes, J.R., Crisp, D., Haberle, R.M., Larsen, S., Magalhaes, J.A., Murphy, J.R., Seiff, A., Wilson, G., 1997. The Mars pathfinder atmospheric structure investigation/meteorology. *Science* 278, 1752–1758.
- Senft, L.E., Stewart, S.T., 2008. Impact crater formation in icy layered terrains on Mars. *Meteoritics & Planetary Science* 43 (12), 1993–2013.
- Shirai, K., Kato, M., Mitani, N.K., Arakawa, M., 2008. Laboratory impact experiments and numerical simulations on shock pressure attenuation in water ice. *Journal of Geophysical Research* 113, 11002.
- Smith, P.H., et al., 2008. Introduction to special section on the Phoenix mission: landing site characterization experiments, mission overviews, and expected science. *Journal of Geophysical Research* 113, E00A18, doi:10.1029/2008JE003083 [printed 114(E3), 2009].
- Stewart, S.T., Ahrens, T.J., 2003. Shock hugoniot of H₂O ice. *Geophysical Research Letters* 30, 65.
- Stewart, S.T., Seifert, A., Obst, A.W., 2008. Shocked H₂O ice: thermal emission measurements and the criteria for phase changes during impact events. *Geophysical Research Letters* 35, 23203.
- Stewart-Mukhopadhyay, S.T., 2002. Collisional processes involving icy bodies in the solar system. Ph.D. Thesis, California Institute of Technology.
- Sutter, B., Ming, D.W., Boynton, W.V., Niles, P.B., Hoffman, J., Lauer, H.V., Golden, D.C., 2009. Summary of results from the Mars Phoenix Lander's thermal evolved gas analyzer. *LPI Contributions* 1502, 29.
- Thompson, S., 1990. ANEOS analytic equations of state for shock physics. Codes input manual. Sandia Report.
- Tosca, N.J., Knoll, A.H., McLennan, S.M., 2008. Water activity and the challenge for life on early mars. *Science* 320, 1204.
- Weibull, W., 1939. A statistical theory of the strength of materials (transl.). *Ingenior Vetenskaps Akademiens Handlingar* 151, 5–45.